Tribology of hard coating alloys deposited by thermal methods: Applications to industrial components

G.E. Carr [1], R.H. Conde *

INTEMA-Div. Soldadura y Fractura-Av. Juan B. Justo 4302 University of Mar del Plata, Argentina

ARTICLE INFO

ABSTRACT

In most of seamless tube making industries, the useful life of mandrels for rotary forging is less than 350 perforation events; though in some cases, the tool may last longer than 1000 perforations. Being the first of a series of hot working steps, improvement during the piercing multiplies the benefits throughout the whole manufacturing process. Mandrels are cast in three metal bases: iron, nickel and cobalt; though lower costs support the use of iron base alloys, mostly when larger mandrel diameters are required. Mandrels lifespan is usually improved by the controlled growth, at high temperature, of a hard oxide film. The research reported in this work is related to the protective oxide films grown on mandrels for seamless tube rotary forging. [2] A laboratory-scale equipment has been entirely designed and built at INTEMA in order to study mandrels wear during the rotary piercing of steel billets. Hard coating oxides grown under a controlled atmosphere on mandrels surface were tested by this equipment, reproducing the wear conditions observed at industrial scale. Wear and oxide film evolution were studied by optical microscopy and energy-dispersive X-ray spectroscopy. Acquired data from lab-scale piercing experiments were analyzed using neural networks (self-organizing maps) to discover relationships among the 22 process parameters and the oxide film characteristics. This method of analysis may well be applied to any industrial component under multivariable hard coating wear conditions.

© 2008 Elsevier B.V. All rights reserved.

1. Introduction

The useful life of mechanical parts in the tube making industry is shortened by wear due to work under severe conditions.

Seamless tubes are made by Mannesmann rotary piercing technique. Round billets are turned into tube shape by means of plastic hot working using a bullet-shaped tool called mandrel.

The aim of the present work is to analyze mandrels wear and thin oxide protective film behaviour at laboratory-scale rotary piercing.

Piercing mandrels are exposed to cyclic thermal shock and friction against steel, during hot working. Three to four mandrels are discarded daily due to wear at TenarisSiderca tube making plant in Argentina. Each worn mandrel had performed from 150 to 350 piercings successfully; though, there have been mandrels that lasted longer than 1600 piercing events. Mandrels are made under strict standards regarding dimensions and chemical composition; however, the reason for such behaviour is still unknown.

The tube making industry is production-oriented, working on a 24-hour-a-day basis. For this reason, scientific research using full scale equipment is not possible. The simultaneous modification of process variables, at the expense of mandrels wear to maintain product dimensions under tolerances, is also common practice. This also affects the systematic study of each process parameter during tube making. For these reasons, a laboratory-scale Mannesmann direct piercer was designed and built (Fig. 1) based on theoretical and practical data found in literature [1–16].

Mandrels wear involves not only material loss but also shape loss; therefore, the model to be designed should also take this fact into account.

Though dimensions change while building a laboratory-scale equipment, material properties do not. The direct piercer laboratory-scale prototype was meant to be a wear study equipment for the comparison of mandrels within the same scale. Data acquired using an ad-hoc designed module were analyzed with neural networks, to discover relationships among variables that could become quantifiers of mandrels wear and factors that might influence it.

Research on mandrels surface by calculus and measuring surface oxide composition by Ohnuki et al. [17] showed that a part of the oxide layer actually reached its melting temperature, acting as a fluid lubricant. This effect was believed to be produced by the thermal flux from the hot worked material into the mandrel in addition to the frictional heat at the interface. Authors stated that temperature

---
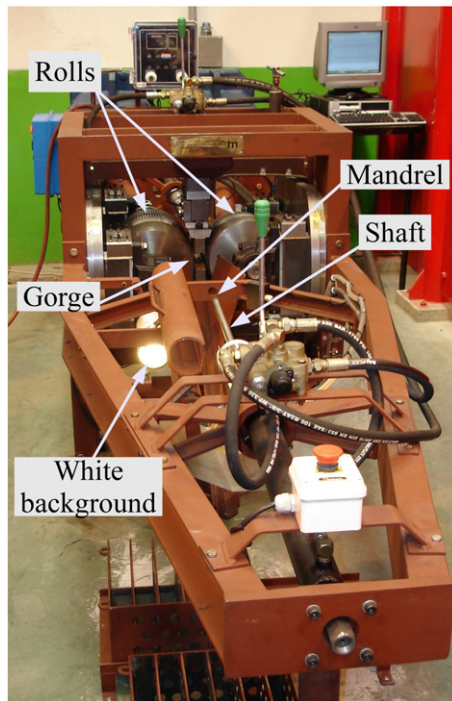
Fig. 1. Laboratory-scale Mannesmann direct piercing wear equipment.

Fig. 2. Mannesmann direct piercing geometry.

reached 900 °C at 50 μm below the oxide film when the external surface temperature had reached 1250 °C. Due to its low heat conductance, the oxide film acted as a thermal barrier.

For the present work the following assumptions were considered:

• The surface oxide film acts as a thermal barrier protecting the underlaying microstructure.
• The oxide layer becomes fluid under shear stresses at high temperature, being this temperature rise due to plastic work and friction between the mandrel and the material.
• A multivariable analysis is necessary to determine those variables critical in the tool's life, and those useful for mandrel wear rate prediction.

The comparison of mandrel behaviours was done once the same series of piercings had been concluded with each mandrel. In this wear tests all but one variable were kept constant.

2. Mannesmann rotary piercing

Mannesmann rotary piercing consists of hot working a round billet by opening a hole at its centre and creating a seamless tube by oblique rolling.

Two barrel-shaped rotating rolls are set side by side leaving a gap between them smaller than the billet diameter. The minimum distance section between the rolls is called gorge. Rolls axes are inclined 4° from the billet axis and rotate in the same direction.

Laboratory-scale direct piercing wear tests were performed by heating up round billets to approximately 1200 °C, then manually inserting them between the piercer rolls. Roll axes warping is responsible for billet axial advance while rotating, resulting in billet surface helical movement. The rod section is reduced in diameter until failure at its centre begins due to plastic collapse provoked by alternating traction and compression stresses (Fig. 2).

The mandrel is positioned at the gorge to open the hole at the section centre. This tool is axially fixed but able to spin freely around its axis. Both mandrel and mandrel shaft are internally water cooled.
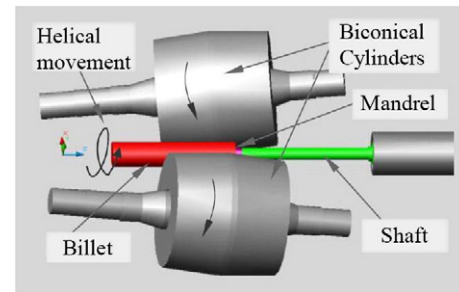
After the rotary piercing event, the hollow remains surrounding the mandrel shaft. The mandrel is axially withdrawn from the gorge and the hollow is removed for later dimensional measurements.

At this position, a digital photograph of the mandrel is taken against a white background, recording its silhouette for further analysis.

The mandrel is then set forth to piercing position for a new perforation event [18].

3. Materials and methods

Parameters kept constant throughout the direct piercing series were the following:

• Geometry and position of rolls, guide shoes, mandrels axial position and shape.
• Billet material (AISI1010 steel), number (20/piercing sequence) and geometry (100 mm long, 38.2 mm diameter).

The mandrel tip is the mostly affected hot working zone, as it is subjected to important thermal loads. This has several consequences:

• Martensite annealing and precipitation of metastable microstructures.
• Generalized plastic deformation with severe grain distortion (Fig. 3).
• Pre-existent oxide layer modification and new layers generation due to billet oxide adherence and mandrel alloy tendency to oxide growth modifies the original thermal barrier characteristics (Fig. 3).

The criterion used for alloys selection and surface treatment of rotary piercing mandrels is cost-based, in comparison with nickel or cobalt based superalloys. Iron based surface treated mandrels have the advantage of continuous growth and restoration of the oxide layer during its lifespan. This oxide layer is useful until temperature rises high enough to decrease bulk metal mechanical yield stress.

Mandrels were made of two alloys, named MT (a 0.2% to 0.3%C, Cr–Ni alloy) and PW (a 0.15%C, Cr–Ni–W alloy) and surface treated at high
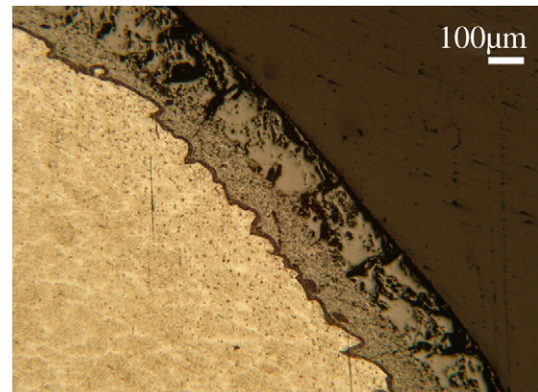

Fig. 3. PW alloy mandrel original oxide layer with billet oxide overlay. Bulk metal grain distortion can also be observed.

Table 1
Mandrels names, alloys and surface treatments

Mandel	Alloy	Surface treatment
B	MT	Conventional
C	PW	PW2
D	PW	PW2
E	PW	PW3
F	PW	PW3

temperature under oxidative atmosphere. Surface treatment for alloy MT is a mixture of industrial furnace combustion exhaust gases, while PW treatments, named PW2 and PW3, are a mixture of gases, mainly nitrogen with the addition of oxygen, carbon dioxide and monoxide, and water vapor in two different proportions. Both alloy compositions and surface treatments are property of TenarisSiderca S.A., therefore exact composition values will not be shown here.

Eleven direct perforation series were performed with MT mandrels and twelve series with PW alloy mandrels.

Six mandrels were analyzed by destructive techniques. Mandrel names, alloys and surface treatments are shown in Table 1.

A non-used MT mandrel and an unaltered PW mandrel zone were taken as references for each alloy undamaged condition. An MT mandrel and four PW mandrels were cut and included in resin for inspection. Six resulting samples were 2% nital etched.

Samples were analyzed using EDS technique (Energy Dispersion Spectroscopy, EDAX-JEOL equipment) to find out observed behaviour with the different oxide layer chemical compositions. These analyses were done by gathering composition percentages from EDS scanning performed along a line across the metal–oxide boundary, starting from bulk metal to oxide film. Aforementioned scans were plotted onto Secondary Electron Images (SEI) for analysis.

Nanoindentation tests were performed in samples of mandrels B (MT) and F (PW3). Analyses were done in both bulk metal and oxide layers, and across bulk metal–oxide interface to find characteristic values of reduced modulus (E_r) and hardness (H) of each alloy and their fluctuation across the oxide–metal boundary. Peak load applied was 7500 μN at 300 μN/s using a Berkovich type indenter with the Triboindenter Hysitron equipment.

After the piercing series, shape variation and volume change were calculated from profiles identified in digital photographs. A set of programs were written in Matlab(R) programming environment for these calculi in order to determine the mandrel that showed the best behaviour.

Data obtained from the direct piercing wear test series were post-processed, from which 22 variables were identified.
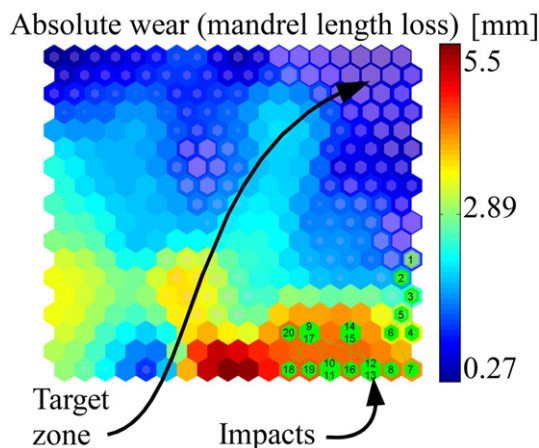
As relationships among these variables were previously unknown, artificial intelligence in the form of self-organizing maps was used to reveal them.

The self-organizing map (SOM) [19–21] is a type of neural network used for mapping high-dimensional data onto a two-dimensional cell array by means of competitive unsupervised learning. An important feature of SOM is that the cell map preserves high-dimensional data topology, making it easier to visualize complex relationships among variables.

Each cell in the map is an *n*-dimensional vector, being '*n*' the number of variables in the data set.

During network training, two steps are followed repeatedly for each input vector in the data set:

1. Find the best-matching unit (a cell whose internal vector is topologically closest to the input vector) using the chosen comparison measurement, such as the euclidean distance.
2. Update the BMU internal vector towards the input vector. The cells which belong to its topological neighborhood in the two-dimensional map grid are also updated likewise.

The number of training stages is proportional to the amount of cells in the map grid. By the end of the training phase, the map grid presents an identical topology to that of the *n*-dimensional data.

After training, the network can be consulted by "impacting" data vectors in their variable maps, in order to detect which cell would become the best-matching unit (BMU) for a given vector.

Kohonen SOM are useful to identify variable combinations associated to different material behaviours, by choosing those variables which could best represent the studied phenomenon.

It must be noted that the topological proximity becomes more meaningful in SOM variable maps than Cartesian axes.

Each cell has a combination of values stored in its internal vector, showed in variable maps, that match those being studied. Hence, when these data impact onto a cell, such place results the same for every map for that piercing event. This is the reason why all variables can be related one to another.

Fig. 4. Self-organizing map for variable 'Absolute wear', target zone (grayed, mostly upper right part of the map) and data impacts for one sequence (mandrel B, green hexagons at low right). (For interpretation of the references to colour in this figure legend, the reader is referred to the web version of this article.)
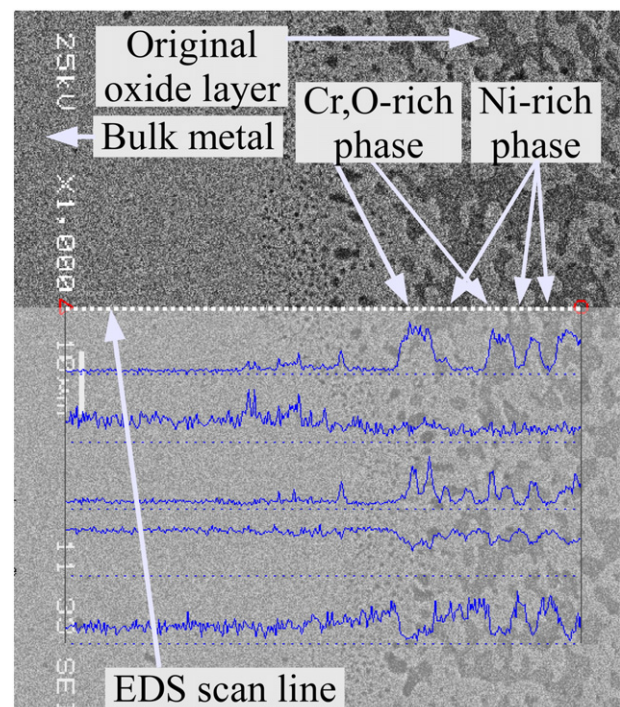

Fig. 5. EDS scan showing dual phase oxide layer (at the right), oxide boundary and base metal (at the left) for mandrel B.
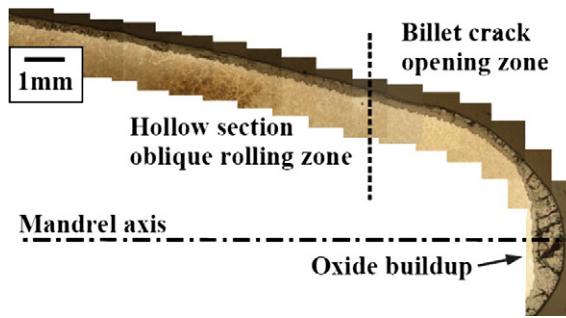
Fig. 6. Oxide built-up zone and thickness profile (mandrel B, MT alloy).

Neighboring cells in the bidimensional network are topologically close to each other in the multidimensional vector space, being this feature called isomorphism.

Twenty two variables were used for network training and to discover relationships among them. Eight variables were found to be the most relevant. Four of them were chosen as input variables because they were laboratory-scale tests process parameters and the other four were chosen as output variables as they accounted directly for mandrels wear.

Input variables:

- Time between piercing events [s]
- Cooling water flow [ml/s]
- Furnace temperature [°C]
- Furnace dwelling time (billet heating time until piercing) [min].

Output variables:

- Axial component work of mandrel friction force [J/mm]
- Electrical motor consumption/billet unit length [KJ/m]
- Mandrel tip spherical radius [mm]
- Absolute wear (mandrel length loss) [mm].

Input variable map values for which minima were found in output variable maps were considered target input values.

In order to determine those input conditions for each alloy to give target values zones on output variables maps, an index to rank mandrels behaviour proximity to ideal was created (Fig. 4).

4. Results

Original mandrel microstructures were identified as martensitic, though annealed martensite was observed at the tool tip zone. Martensitic microstructure is the result of mandrel alloys and the high cooling rate of the casting process.

A dual phase oxide layer was observed in all mandrels used for wear tests.
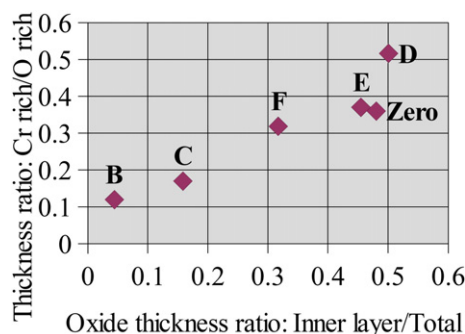

Fig. 7. Correlation between EDS composition profiles scan and oxide thickness measurements done by metallograpy.

Table 2
Chromium content in the original oxide layer and oxide thickness increase factor at PW alloy mandrels tip (final total oxide thickness/original oxide thickness)

Mandrel	Cr content [%]	Mandrel tip oxide total thickness increase factor
C	1.07	3.69
D	1.61	3.25
E	1.81	1.43
F	2.72	1.25

A 100 μm thick, intergranular grown oxide layer was observed in MT alloy mandrels after surface treatment and prior to direct piercing wear tests. This layer was coherent with the bulk metal.

Oxide total thickness was approximately 250 μm. A higher chromium content was detected in the oxide at the zone adjacent to the bulk metal. This zone was 85 μm thick.

Due to the fact that oxide in the rear part of the mandrels was not modified by the piercing wear process, it was decided to take these zones as reference for oxide and microstructure original conditions.

Oxide original microstructure was dual-phased. The characteristic dimension for these phases was 5 μm.

In each composition scanned by EDS, one phase was observed to be chromium and oxygen rich while the other was found to be nickel rich (Fig. 5).

It was also observed that, in the oxide layer, the alloy-rich precipitate size increased at the mandrel tip. The characteristic dimension of these precipitants is 10 μm at the outer layer decreasing to 1 μm at the oxide boundary with bulk metal (Fig. 5).

Adhesion of iron oxide from billet to mandrel surface was observed for all wear tests. This was determined after discovering a uniform oxide layer without any alloy element on top of the original oxide layer. This oxide layer showed a maximum thickness at the mandrel tip and zero at the rear part (Fig. 6).

Relative thicknesses of chromium rich oxide layers were plotted against total thicknesses, measured on micrographies. The internal oxide layer seen on micrographies is in agreement with the alloy-rich layer as seen on EDS scanning counts (Fig. 7). These data were obtained measuring oxide layer thicknesses in optical micrographies and comparing them to those measured in EDS scans plotted onto SEI imaging.

In PW alloy samples, it was also observed that, after direct piercing wear tests, the oxide thickness increase was inversely proportional to the chromium concentration in the inner layer of oxide, i.e., the original oxide layer grown by surface treatment.

Chromium concentrations in the original oxide precipitates as well as oxide thickness increase factors at mandrel tip zone are shown in Table 2.

Reduced modulus and hardness measurements were made in zones in the bulk 80 μm near the boundary, affected by surface treatment, and unaffected zones of base metal. Corresponding values are shown in Table 3. These data were calculated by averaging 9 measurements made in 3 by 3 indentation square grids, 4 μm side length.

Nanoindentation tests on mandrel B (MT) showed that reduced modulus as well as hardness increased along a path in the base metal starting at 50 μm below the oxide layer towards the bulk (Fig. 8).

Table 3
Reduced modulus and hardness of the mandrels bulk metal far from oxide layer and 80 μm below the oxide boundary as measured by nano indentation tests

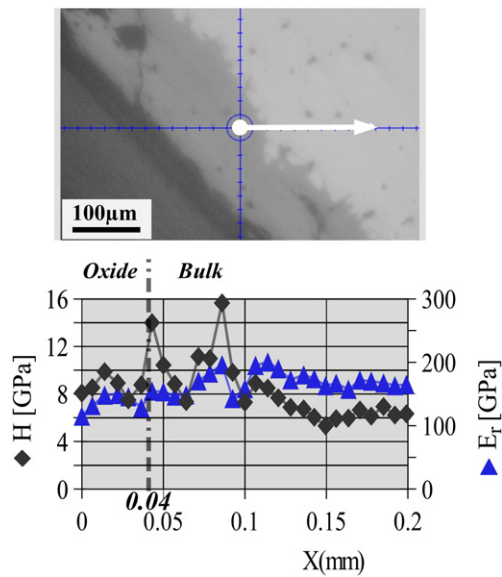|	Near boundary		Bulk	
	E_r [GPa]	H [GPa]	E_r [GPa]	H [GPa]
B original	166.6±3.7	6.4±0.3	178.5±11.0	8.45±1.1
B tip	118.3±3.3	7.2±0.6	158.8±2.9	7.7±0.3
F original	131.9±4.8	8.5±0.8	166.9±13.8	6.9±0.9
F tip	118.8±1.5	7.7±0.2	175.9±6.5	10.6±0.6

Fig. 8. Nanoindentation test results across mandrel B oxide boundary. White arrow length shows path in optical micrography.

On mandrel F (PW3) an increase in hardness was observed while moving away from oxide boundary to mandrel bulk near the tip. Near the original oxide at the rear part of the mandrel, the opposite situation was observed (Fig. 9). This fact could be associated to the presence of Cr–W carbide in non-annealed martensite.

Hardness profile values were measured along a line from built-up oxide to inside the base metal. In F mandrel, observed values increase to double from built-up oxide to original oxide at 50 μm outside the oxide boundary, while in mandrel B this hardness increase is observed approximately 50 μm inside the oxide–metal interface.

Reduced modulus (E_r) values are slightly higher in gained oxide, lowering smoothly with depth towards bulk material for mandrel F while for mandrel B they were similar at both sides.
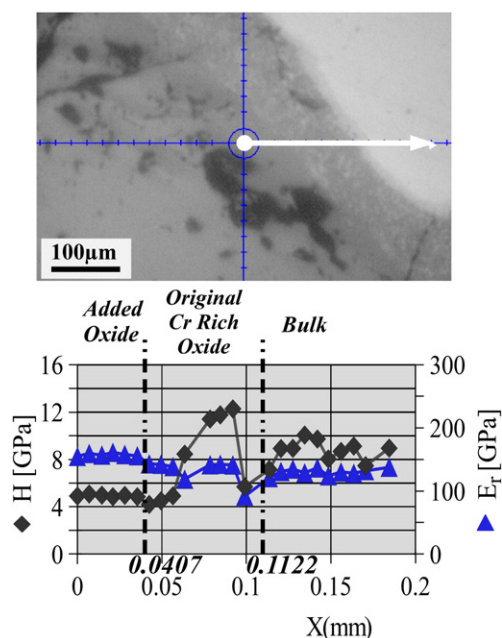

Fig. 9. Nanoindentation tests along a line across mandrel F oxide boundary. White arrow length shows path in optical micrography.

Table 4
Mandrels wear beahviour ranking

Mandel	Index
F	0.2463
E	0.1254
D	0.1220
B	0.0805
C	0.0743

Self-organizing maps (SOM) analysis showed that many variables exhibited similar behaviour. These relationships helped in understanding the piercing process.

Furnace temperature and cooling water flow variables importance on axial mandrel force was established by observing a proportional variation between them.

A direct relationship was found between the spherical mandrel tip radius and absolute wear (mandrel length loss).

Mandrels behaviour impacts on output variables target maps were ranked as shown on Table 4. Mandrel F showed the best wear resistance, followed by mandrels E, D, B and C.

5. Discussion

The original oxide layer must have a minimum thickness of 60 μm to ensure that bulk metal temperature remains lower than 1100 °C, above which the mechanical properties loss takes place. In spite of this, bulk metal resistance to deformation can be lowered if local temperature increase is provoked by high deformation velocities near the mandrel surface. Since oxide acts as a thermal barrier, an excessive thickness of this layer might be detrimental due to oxide overheating and melting [18], which would in turn increase the local heat transfer coefficient.

It can be seen that, for every mandrel studied along the present work, temperature has surpassed that limit and severe plastic deformation was detected in the form of shape loss.

Once mandrel bullet-like shape is lost, redundant deformation takes place at billet material close to the mandrel surface, leading to local temperature rise and, again, shape loss increases. This leads to an increase of the oxide deposit thickness at the mandrel tip area.

The oxide layer at the rear part of mandrels remains unaltered after direct piercing series. This is because hot working is performed mostly by the mandrel tip and its middle section. This fact was confirmed by comparing metallographies taken from mandrel Zero, MT without wear, and mandrel B (MT). Such an unaltered zone, distant from mandrel tip, is also recognizable by the non-annealed martensite microstructure underneath the oxide layer. Therefore, those mandrel regions were used as reference of the original oxide microstructure condition.

By matching analysis results made by EDS technique to SOM analysis results of mandrels wear behaviour, it can be said that the chromium concentration in the original oxide layer may have a major importance in wear resistance, as this property turned out to be inversely proportional to chromium percentage.

Taking into account that there is a relatively high hardness zone in the original oxide layer of PW mandrels and the same high hardness zone was observed at 50 μm deep inside the base metal, it is proposed that the first of these two conditions is the best against high temperature mandrels wear. The oxide film may act as a high resistance zone as well as a thermal barrier, protecting the bulk metal. In MT alloy mandrels, the aforementioned zone was located inside the base metal; for that reason it is believed to be the cause of the bad behaviour against wear, due to overheating and the leading cause to plastic deformation of the base layer.

Shape loss due to these simultaneous causes contribute to mandrel tip radius increase and, as a consequence, to the rising of friction against the hot worked material.

An Eq. (1) describing mandrels wear is proposed as a starting point for further research.

$$f_{Wear}(D_{Absolute}, rad_m)) \propto \frac{A \cdot B}{C} \cdot D \tag{1}$$

being:

A $K_1 \cdot f_1 (t_{bp}, T_F)$
B $K_2 \cdot W_{Fr} (t_F, qH_2O)$
C $K_3 \cdot f_2 (\varphi_{Rod})$
D $K_1 \cdot f_4 \left(\frac{K_{TOx}}{\%Cr_{Ox}, H_{Ox}, \overline{X}_{maxH}, e_{Ox}} \right)$

where:

f_{Wear} is a complex function (a kind of weighted addition of the variables $D_{absolute}$, 'Absolute wear', and rad_m, 'Mandrel tip radius').

A   accounts for the influence of 'Furnace temperature' and t_{bp}, 'Time between piercing events'.

B   accounts for the influence of 'Axial component work of mandrel friction force', which depends directly on t_F, 'Furnace dwelling time' and qH_2O, 'Cooling water flow'.

C   accounts for the influence of the billet diameter, Φ_{Rod}, which also depends on furnace dwelling time, though not shown.

D   considers the tribological interphase phenomena, described by metallurgical variables related to the mandrel: K_{TOx} is the oxide thermal coefficient, $\%Cr_{Ox}$ is the chromium percentage at the dual phase oxide layer, H_{Ox} is the oxide layer hardness peak, X_{maxH} is the position of the oxide hardness peak, related to metal–oxide boundary and e_{Ox} is the oxide thickness.

6. Conclusions

Laboratory-scale Mannesmann rotary piercing wear tests were performed on 22 mandrels. From these tests experimental numerical data has been acquired. Five used mandrels were cut and analyzed using metallographic, EDS and nanoindentation techniques.

A self-organizing map was trained with acquired data to determine useful variables and relationships and to relate mandrels surface conditions to mandrels wear resistance ranking. This ranking was determined by the creation of target zones coincident with wear indicative variables minima. Input variables according to process pre-set parameters were analyzed and the following ranges for output optimum values arose:

• Time between piercing events:	50±5 s
• Cooling water flow:	7±0.5 ml/s
• Furnace temperature:	1206±5°C
• Furnace dwelling time:	340±20 min.

Mandrels with PW3 alloy showed the best wear behaviour while MT alloy mandrels were the most damaged.

From analysis discussed before, we can conclude that the oxide layer characteristics are important to wear resistance. Chromium content in original oxide revealed as the most important factor responsible of the existence of a relatively high hardness zone 50 μm outside the oxide boundary. This discovery was not reported previously in literature.

SOM variables maps data analysis method should be applicable to new different conditions and variables for these wear tests, i.e., mandrel axial position, rolls axis warping angle, gorge diameter, etc.

Furthermore, SOM analysis technique can be performed with data obtained from microstructural thin films nanoscopic analysis.

Finally, this method of analysis may well be applied to full scale wear processes, as well as to different pieces of steel making components, by choosing the appropriate variables and criteria.

References

[1] F. Brisotto, R. Bedogni, L. Montelatici, E. Ceretti, C. Giardini, International Conference in Innovation in Metal Forming (Brescia, Italy, 2004.
[2] E. Cavaleri, D. Tormo, J. Brandaleze, JORNADAS SAM/CONAMET/SIMPOSIO MATERIA 2003, p.238–241, Sociedad Argentina de Materiales, 2003, pp. 04–19.
[3] C. Attanasio, A. Brisotto, F. Ceretti, E. Giardini, VI A.I.Te.M., Gaeta, Universitá di Brescia, Italia, 2003.
[4] E. Erman, J. Mech. Work. Technol. 15 (1987) 167.
[5] F. Kocks, Stahl und Eisen 47 (1927) 443.
[6] E.I. Panov, Metallurgist 49 (7–8) (2005) 280.
[7] R. Siebel, Stahl und Eisen 47 (1927) 1685.
[8] V.S. Smirnov, Stal-Metallurgizdat (1953) 756.
[9] H. Cmupneof, Mechanical Engineering Information 3 (1955) 49.
[10] Yu. F. Teterin, P.K. Luzin, Stal-Metallurgizdat 930 (1960).
[11] I.M. Blazynski, T.Z. Cole, Proceedings of the Institution of Mechanical Engineers 178 (1963–64) 867.
[12] I.A. Fomichev, Stal-Metallurgizdat (1958) 176.
[13] T. Shimizu, N. Morioka, H. Oka, Kawasaki Steel Report 38 (1998) 38.
[14] F. Togashi, A. Ejima, H. Abe, Y. Funyu, K. Sakurada, T. Maguchi, Y. Tagu, Y. Sayama, Kawasaki Steel Technical Report 4 (1981).
[15] N. Konya, Y. Hayashi, H. Oka, T. Imae, Y. Funyu, T. Okumura, Kawasaki Steel Technical Report 16 (1987) 31.
[16] K. Osakada, K. Mori, H. Yoshimura, J. Mater. Process. Technol. 80–81 (1998) 700.
[17] K. Ohnuki, A. Hamazu, S. Kawanami, T. Nakajima, Iron and Steel Institute of Japan 72 (1986) 450.
[18] G.E. Carr PhD Thesis. "Caracterización Tribológica y Desgaste de Materiales para la Industria Siderúrgica", Universidad Nacional de Mar del Plata, Argentina, 2008.
[19] T. Kohonen, Biol. Cybern. 43 (1) (1982) 59.
[20] T. Kohonen, Proc. IEEE, vol. 78, 1990, pp. 1464–1480.
[21] T. Kohonen, 1st ed., Self-Organizing Maps, vol. 30, Springer Series in Information Sciences, 1995.